JPB CAC

CORRESPONDENCE
AS OF

June 16, 2020

Givens, Patrice

From: Thomas Weissmiller <tarzantom@astound.net> on behalf of tarzantom@pobox.com
Sent: Wednesday, May 20, 2020 7:29 PM
To: cacsecretary [@caltrain.com]
Subject: Question on Grade Crossing Solutions, E. Bellevue Ave, San Mateo

I made a public comment on the above during the May 20th Citizens Advisor Committee, Item #7. Joe Navarro said he would look in to it.

Below is a picture of the lane divider on E. Bellevue in San Mateo. Not sure if they add safety value.

I drive this street often. These dividers used to have a short pole with a reflector. These are often hit. In this picture they do not have the reflector. Maybe they are not being replaced anymore.

IMHO they do not reduce the risk of head on collisions. They do hinder a driver who might try to beat a down crossing, but the chance of this happening seems extremely remote.

If these dividers are going to remain, they need to be more visible to drivers.

If there is no data that supports the need for these dividers at this location and there are no regulatory requirements, I suggest they be removed.

Tom

Thomas Weissmiller (Weißmüller)
San Mateo, CA : Cell: 650-218-6386 : Reply to tarzantom@pobox.com

Givens, Patrice

From: Roland Lebrun <ccss@msn.com>
Sent: Thursday, May 21, 2020 5:08 AM
To: VTA Board Secretary
Cc: Board (@caltrain.com); SFCTA Board Secretary; MTC Commission; cacsecretary [@caltrain.com]; SFCTA CAC
Subject: A&F item 14 Caltrain sales tax

Dear Chair Carr,

I am respectfully requesting deferral of your approval of the San Mateo County Transit District's (AKA "SamTrans") request for support of a 1/8 cent sales tax for Caltrain for the following reasons:

1. This Measure will not go on the November ballot for the same reason that the Faster Bay Area and $10B housing bond measures will not go on the ballot either.
2. A deferral would give us a unique opportunity to mandate changes of Caltrain management whose incompetence is exacerbating the financial crisis triggered by COVID.
3. Last but not least, VTA staff's assertion that this Measure *"will relieve VTA's operating budget of the formula share of our contribution to Caltrain operations and capital (Budgeted for FY2021 at $10.8 million operating and $5 million capital)"* constitutes a potential violation of the 2000 Measure A as approved by the voters of Santa Clara County which could be subject to legal challenge.

Funding operating and maintenance costs for increased bus, rail and paratransit services
"Provide revenue to ensure funding, to at least 2014, and possibly longer, of the following: the new Tasman East, Capitol and Vasona Light Rail Lines, ***the commuter rail connection to BART****"*

Sincerely,

Roland Lebrun

cc
Caltrain Board
SFCTA Commissioners
MTC Commissioners
SFCTA CAC
Caltrain CAC
VTA CAC

Givens, Patrice

From: Roland Lebrun <ccss@msn.com>
Sent: Tuesday, May 26, 2020 2:14 AM
To: Board (@caltrain.com)
Cc: SFCTA Board Secretary; VTA Board Secretary; MTC Info; SFCTA CAC; cacsecretary [@caltrain.com]
Subject: Finance Committee #6 Statement of revenues and expenses
Attachments: March 2020 Revenues and Expenses.pdf; April 2020 Revenues and Expenses.pdf

Dear Chair Davis and Board members,

Here are my written comments for item #6 April 2020 revenue and expenses

Line 1 Farebox Revenue dropped from a $2.2M (3%) surplus to a $5.4M (6.4%) deficit.
Question through the chair: **What have staff done in the last 2 months to flatten the freefall**?

Line 23 Rail operator service shows a slight decrease over last month but it is not proportional with the catastrophic reduction in service.

Line 38 Wages and benefits:
Question through the chair: **Why hasn't there been any reduction in wages and benefits through furloughs and/or pay cuts and the elimination of overtime?**

Line 41 Professional Services:
Question through the chair: **How could Professional Services possibly have increased by $1.1M (25% of the entire annual budget) in a single month?**

The $19M increase in reserves (from $84M on 3/31 to $103M on 4/30) probably reflects the $43M in CARES revenues and must be monitored carefully.

Please refer to the attached March and April 2020 statements for additional information.

Sincerely,

Roland Lebrun

cc
SFCTA Commissioners
VTA Board of Directors
MTC Commissioners
SFCTA CAC
Caltrain CAC

PENINSULA CORRIDOR JOINT POWERS BOARD

STATEMENT OF REVENUE AND EXPENSE

Fiscal Year 2020

March 2020

				% OF YEAR ELAPSED		75.0%	
	YEAR TO DATE					ANNUAL	
	PRIOR ACTUAL	CURRENT ACTUAL	$ VARIANCE	% VARIANCE	CURRENT AS A % OF BUDGET	APPROVED BUDGET	
REVENUE							
OPERATIONS:							
Farebox Revenue	74,400,004	76,658,628	2,258,624	3.0%	72.3%	106,000,000	1
Parking Revenue	3,831,796	3,613,331	(218,465)	(5.7%)	67.7%	5,335,000	2
Shuttles	1,442,525	1,426,910	(15,615)	(1.1%)	57.0%	2,503,200	3
Rental Income	1,418,873	1,473,634	54,761	3.9%	71.5%	2,060,540	4
Other Income	1,867,405	2,589,865	722,460	38.7%	147.7%	1,753,450	5
							6
TOTAL OPERATING REVENUE	82,960,602	85,762,367	2,801,765	3.4%	72.9%	117,652,190	7
							8
CONTRIBUTIONS:							9
AB434 Peninsula & TA Shuttle Funding	1,296,368	1,487,583	191,215	14.8%	85.6%	1,737,950	10
Operating Grants	4,927,955	3,897,194	(1,030,762)	(20.9%)	73.2%	5,327,497	11
JPB Member Agencies	20,523,500	23,296,918	2,773,418	13.5%	77.9%	29,921,971	12
Use of Reserves	-	-	-	0.0%	0.0%	1,064,614	13
							14
TOTAL CONTRIBUTED REVENUE	26,747,823	28,681,694	1,933,871	7.2%	75.4%	38,052,032	15
							16
GRAND TOTAL REVENUE	**109,708,425**	**114,444,062**	**4,735,636**	**4.3%**	**73.5%**	**155,704,222**	17
							18
							19
EXPENSE							20
							21
OPERATING EXPENSE:							22
Rail Operator Service	63,459,048	66,721,859	3,262,811	5.1%	73.5%	90,817,696	23
Positive Train Control	20,481	213,740	193,259	943.6%	8.9%	2,400,000	24
Security Services	4,018,753	4,362,804	344,050	8.6%	66.7%	6,544,183	25
Shuttles Services	2,945,062	3,017,105	72,044	2.4%	57.0%	5,290,100	26
Fuel and Lubricants	7,893,520	7,991,869	98,349	1.2%	72.6%	11,003,417	27
Timetables and Tickets	54,175	57,539	3,363	6.2%	40.1%	143,500	28
Insurance	3,150,288	3,244,061	93,772	3.0%	72.0%	4,506,064	29
Claims, Payments, and Reserves	333,088	(90,702)	(423,790)	(127.2%)	(9.5%)	951,794	30
Facilities and Equipment Maint	1,419,345	1,683,690	264,344	18.6%	50.4%	3,339,391	31
Utilities	1,359,644	1,430,640	70,996	5.2%	68.0%	2,105,422	32
Maint & Services-Bldg & Other	730,496	996,912	266,416	36.5%	63.6%	1,567,930	33
							34
TOTAL OPERATING EXPENSE	**85,383,901**	**89,629,515**	**4,245,614**	**5.0%**	**69.7%**	**128,669,496**	35
							36
ADMINISTRATIVE EXPENSE							37
Wages and Benefits	7,769,122	8,959,177	1,190,055	15.3%	74.3%	12,061,633	38
Managing Agency Admin OH Cost	5,192,071	3,189,361	(2,002,710)	(38.6%)	62.6%	5,098,065	39
Board of Directors	15,634	9,966	(5,669)	(36.3%)	68.3%	14,600	40
Professional Services	1,527,730	2,680,962	1,153,232	75.5%	62.7%	4,275,583	41
Communications and Marketing	193,514	224,670	31,156	16.1%	74.5%	301,500	42
Other Office Expenses and Services	2,381,970	1,783,169	(598,801)	(25.1%)	67.5%	2,643,572	43
							44
TOTAL ADMINISTRATIVE EXPENSE	**17,080,041**	**16,847,304**	**(232,737)**	**(1.4%)**	**69.1%**	**24,394,953**	45
							46
Long Term Debt Expense	886,412	2,018,290	1,131,877	127.7%	76.5%	2,639,773	47
							48
GRAND TOTAL EXPENSE	**103,350,355**	**108,495,109**	**5,144,754**	**5.0%**	**69.7%**	**155,704,222**	49
							50
NET SURPLUS / (DEFICIT)	**6,358,071**	**5,948,953**	**(409,118)**	**(6.4%)**		**(0)**	51

4/10/20 6:36 PM

PENINSULA CORRIDOR JOINT POWERS BOARD

INVESTMENT PORTFOLIO

AS OF MARCH 31, 2020

TYPE OF SECURITY		MATURITY DATE	INTEREST RATE	PURCHASE PRICE	MARKET RATE
Local Agency Investment Fund (Unrestricted)	*	Liquid Cash	1.787%	40	40
County Pool (Restricted)		Liquid Cash	1.776%	624,073	624,073
Other (Unrestricted)		Liquid Cash	0.700%	68,820,359	68,820,359
Other (Restricted)	**	Liquid Cash	0.200%	14,626,183	14,626,183
				$ 84,070,655	$ 84,070,655

Interest Earnings for March 20	$ 32,777.41
Cumulative Earnings FY2020	$ 301,815.88

* The market value of Local Agency Investment Fund (LAIF) is calculated annually and is derived from the fair value factor as reported by LAIF for quarter ending June 30th each year.

** Prepaid Grant funds for Homeland Security, PTMISEA and LCTOP projects, and funds reserved for debt repayment. The Portfolio and this Investment Report comply with the Investment Policy and the provisions of SB 564 (1995). The Joint Powers Board has the ability to meet its expenditure requirements for the next six months.

PENINSULA CORRIDOR JOINT POWERS BOARD

STATEMENT OF REVENUE AND EXPENSE

Fiscal Year 2020

April 2020

				% OF YEAR ELAPSED	83.3%		
	YEAR TO DATE					ANNUAL	
	PRIOR ACTUAL	CURRENT ACTUAL	$ VARIANCE	% VARIANCE	CURRENT AS A % OF BUDGET	APPROVED BUDGET	
REVENUE							
OPERATIONS:							
1 Farebox Revenue	84,793,550	79,348,545	(5,445,006)	(6.4%)	74.9%	106,000,000	1
2 Parking Revenue	4,417,731	3,655,591	(762,140)	(17.3%)	68.5%	5,335,000	2
3 Shuttles	1,632,850	1,670,612	37,761	2.3%	66.7%	2,503,200	3
4 Rental Income	1,568,094	1,956,714	388,620	24.8%	95.0%	2,060,540	4
5 Other Income	2,143,230	2,809,059	665,828	31.1%	160.2%	1,753,450	5
6							6
7 TOTAL OPERATING REVENUE	94,555,456	89,440,520	(5,114,936)	(5.4%)	76.0%	117,652,190	7
8							8
9 CONTRIBUTIONS:							9
10 AB434 Peninsula & TA Shuttle Funding	1,440,488	2,115,793	675,306	46.9%	121.7%	1,737,950	10
11 Operating Grants	5,475,506	4,335,253	(1,140,253)	(20.8%)	81.4%	5,327,497	11
12 JPB Member Agencies	22,165,000	25,104,921	2,939,921	13.3%	83.9%	29,921,971	12
13 Use of Reserves	-	-	-	0.0%	0.0%	1,064,614	13
14							14
15 TOTAL CONTRIBUTED REVENUE	29,080,993	31,555,967	2,474,974	8.5%	82.9%	38,052,032	15
16							16
17 **GRAND TOTAL REVENUE**	**123,636,450**	**120,996,487**	**(2,639,963)**	(2.1%)	77.7%	**155,704,222**	17
18							18
19							19
20 **EXPENSE**							20
21							21
22 OPERATING EXPENSE:							22
23 Rail Operator Service	70,571,335	73,460,584	2,889,249	4.1%	80.9%	90,817,696	23
24 Positive Train Control	34,988	344,375	309,387	884.3%	14.3%	2,400,000	24
25 Security Services	5,289,405	4,872,062	(417,343)	(7.9%)	74.4%	6,544,183	25
26 Shuttles Services	3,300,159	3,349,034	48,875	1.5%	63.3%	5,290,100	26
27 Fuel and Lubricants	8,672,856	8,265,007	(407,849)	(4.7%)	75.1%	11,003,417	27
28 Timetables and Tickets	87,245	58,099	(29,147)	(33.4%)	40.5%	143,500	28
29 Insurance	3,498,105	3,605,396	107,291	3.1%	80.0%	4,506,064	29
30 Claims, Payments, and Reserves	599,870	(69,829)	(669,699)	(111.6%)	(7.3%)	951,794	30
31 Facilities and Equipment Maint	1,763,869	1,900,378	136,509	7.7%	56.9%	3,339,391	31
32 Utilities	1,571,427	1,571,664	237	0.0%	74.6%	2,105,422	32
33 Maint & Services-Bldg & Other	786,037	1,117,688	331,651	42.2%	71.3%	1,567,930	33
34							34
35 TOTAL OPERATING EXPENSE	**96,175,296**	**98,474,458**	**2,299,162**	2.4%	76.5%	**128,669,496**	35
36							36
37 ADMINISTRATIVE EXPENSE							37
38 Wages and Benefits	8,520,172	9,873,027	1,352,854	15.9%	81.9%	12,061,633	38
39 Managing Agency Admin OH Cost	5,805,634	3,598,588	(2,207,046)	(38.0%)	70.6%	5,098,065	39
40 Board of Directors	16,795	10,024	(6,770)	(40.3%)	68.7%	14,600	40
41 Professional Services	1,896,116	3,789,504	1,893,389	99.9%	88.6%	4,275,583	41
42 Communications and Marketing	230,395	239,720	9,325	4.0%	79.5%	301,500	42
43 Other Office Expenses and Services	2,704,408	1,560,402	(1,144,006)	(42.3%)	59.0%	2,643,572	43
44							44
45 TOTAL ADMINISTRATIVE EXPENSE	**19,173,520**	**19,071,266**	**(102,253)**	(0.5%)	78.2%	**24,394,953**	45
46							46
47 Long Term Debt Expense	886,412	2,186,864	1,300,452	146.7%	82.8%	2,639,773	47
48							48
49 **GRAND TOTAL EXPENSE**	**116,235,228**	**119,732,589**	**3,497,361**	3.0%	76.9%	**155,704,222**	49
50							50
51 **NET SURPLUS / (DEFICIT)**	**7,401,222**	**1,263,899**	**(6,137,323)**	(82.9%)		(0)	51

PENINSULA CORRIDOR JOINT POWERS BOARD

INVESTMENT PORTFOLIO

AS OF APRIL 30, 2020

TYPE OF SECURITY		MATURITY DATE	INTEREST RATE	PURCHASE PRICE	MARKET RATE
Local Agency Investment Fund (Unrestricted)	*	Liquid Cash	1.648%	36,574	36,574
County Pool (Restricted)		Liquid Cash	1.622%	548,903	548,903
Other (Unrestricted)		Liquid Cash	0.700%	90,036,432	90,036,432
Other (Restricted)	**	Liquid Cash	0.200%	12,425,057	12,425,057
				$ 103,046,966	$ 103,046,966

Interest Earnings for April 20	$ 56,392.81
Cumulative Earnings FY2020	$ 358,208.69

* The market value of Local Agency Investment Fund (LAIF) is calculated annually and is derived from the fair value factor as reported by LAIF for quarter ending June 30th each year.

** Prepaid Grant funds for Homeland Security, PTMISEA and LCTOP projects, and funds reserved for debt repayment. The Portfolio and this Investment Report comply with the Investment Policy and the provisions of SB 564 (1995). The Joint Powers Board has the ability to meet its expenditure requirements for the next six months.

Givens, Patrice

From: Jeff Carter <jcartrain@aol.com>
Sent: Friday, May 29, 2020 11:26 AM
To: cacsecretary [@caltrain.com]
Cc: JCARTRAIN@aol.com; Navarro, Joe
Subject: Please Forward To CAC Chair Brian Shaw--Distance-Based Fares

Good Morning Brian,

The JPB CAC Work Plan shows distance-based fares scheduled for the June 17, 2020 Meeting.

Since I have been advocating for this, as has Adrian Brandt, would it be helpful to discuss this along with staff in order to provide an in-depth staff report to help CAC members and the public better understand how Caltrain can implement a distance-based fare system?

I have developed a distance-based fare matrix for Caltrain.

Thank-You,

Jeff Carter

(925) 207-3408

Givens, Patrice

From: Seamans, Dora
Sent: Tuesday, June 02, 2020 4:54 PM
To: Board (@caltrain.com); cacsecretary [@caltrain.com]
Subject: Emailing - Approved_BAC Chair Letter_Caltrain Corridor Slow Streets (004).pdf
Attachments: Approved_BAC Chair Letter_Caltrain Corridor Slow Streets (004).pdf

Hello – please find the attached correspondence received from the Caltrain Bicycle Advisory Committee addressed to the Peninsula Corridor Joint Powers Board and Caltrain Citizens Advisory Committee.

Best,

Dora

Dora Seamans, MPA, CMC
Executive Officer/District Secretary
SamTrans, Executive Administration
1250 San Carlos Ave
San Carlos, CA 94070
Tel: 650-508-6242
Seamansd@samtrans.com

May 21, 2020

Peninsula Corridor Joint Powers Board
Caltrain Citizens Advisory Committee
1250 San Carlos Ave.
San Carlos, CA 94070

A Proposal for "Slow Streets" for Bicycling and Walking Along the Caltrain Corridor

Dear Peninsula Corridor Joint Powers Board and Caltrain Citizens Advisory Committee,

As you are aware Caltrain has seen a precipitous drop in ridership since our local county shelter in place orders went into effect in March, with ticket sales dropping by 95%. While we hope that our collective success in flattening the curve will lead to a rebound over the course of the summer and fall there is still much uncertainty in how soon riders will return to Caltrain and other public transit.

Ordinarily we would reach out to local jurisdictions to encourage improving connections for biking to and from individual Caltrain stations. This work is still important and we hope to see it continue. Right now the need is even greater to facilitate bicycle trips between destinations along the corridor that might normally be taken by train. As businesses reopen and residents gradually return to work and other destinations it's crucial that viable alternatives to driving be made available. Given that the estimated average (mean) trip was 22.9 miles in 2019 it's likely that a substantial number of trips could be substituted on a bicycle or e-bike, particularly during the dry summer months. Routes like Old County Road in Belmont and San Carlos and Evelyn Avenue in Mountain View and Sunnyvale could be made more enticing so that typical train commuters feel safe riding a bike instead of driving.

We applaud the jurisdictions along the Caltrain Corridor who have already begun some sort of "slow streets" program to enable more people to safely walk and bike. But we would like to see this taken a step further - jurisdictions must work with their neighboring cities and counties to make sure that there are safe bike routes up and down the Peninsula and through the South Bay.

Sincerely,
The Caltrain Bicycle Advisory Committee

Cc: San Francisco Board of Supervisors, Municipal Transportation Agency, Mayor London Breed, BAC
San Mateo County Board of Supervisors, County BPAC, CCAG BPAC
Brisbane City Council and Complete Streets Committee
South San Francisco City Council and BPAC
San Bruno City Council and BPAC
Millbrae City Council and Parks and Recreation Committee

Burlingame City Council and Traffic Safety and Parking Commission
San Mateo City Council and Sustainability and Infrastructure Commission
Belmont City Council and Parks and Recreation Commission
San Carlos City Council and Transportation & Circulation Committee
Redwood City Council and Complete Streets Committee
Atherton City Council and BPAC
Menlo Park City Council and Complete Streets Commission
Santa Clara County Board of Supervisors
Palo Alto City Council and BPAC
Mountain View City Council and BPAC
Sunnyvale City Council and BPAC
Santa Clara City Council and BPAC
San Jose City Council and BPAC
Morgan Hill City Council and BPAC
Gilroy City Council and BPAC

Givens, Patrice

From: Adrian Brandt <adrian.brandt@gmail.com>
Sent: Wednesday, June 10, 2020 1:37 PM
To: Navarro, Joe; cacsecretary [@caltrain.com]
Subject: New 70-train skp-stop schedule asymmetry?

Regarding the new 70-train weekday "skip-stop" schedule:

Why is skip-stop service oddly asymmetric for the very popular mid-line Redwood City station?

It's an "all-trains-stop" station only for AM southbound trains, while it's a skipped-stop for all other peak train directions.

Millbrae and Mountain View also have similar asymmetries regarding which peak train directions they are either served by all trains or skipped by some.

Givens, Patrice

From: Roland Lebrun <ccss@msn.com>
Sent: Friday, June 12, 2020 3:10 AM
To: BART Board
Cc: SFCTA Board Secretary; MTABoard@SFMTA.com; Board (@caltrain.com); VTA Board Secretary; MTC Info; cacsecretary [@caltrain.com]; SFCTA CAC; cac@sfmta.com
Subject: Real-time COVID detectors

Dear President Simon and Board members,

Thank you for the opportunity to address you verbally during yesterday's Board meeting.
The intent of this email is to substantiate and elaborate on the comments I made about Airborne Virus Detectors (AVDs).

Background

- BART and other transit agencies are already working on measures to counteract a CDC recommendation to avoid public transit because social distancing is not always effective in enclosed spaces requiring forced ventilation.
- BART and other agencies have correctly identified that UV filtration is key to the restoration of public confidence in mass transportation.

Airborne Virus Detectors (AVDs)

Unlike UV filtration systems, AVDs are passive devices:
https://www.nature.com/articles/srep17462

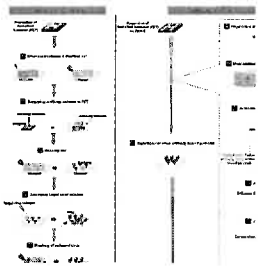

Detection of airborne viruses using electro-aerodynamic deposition and a field-effect transistor | Scientific Reports

We report a technique for the detection of aerosolized viruses. Conventional field-effect-transistor (FET)-based techniques use solution-based processes, thus require antibody binding to the ...

www.nature.com

https://www.sciencedaily.com/releases/2020/04/200421112520.htm

The proposal

The proposal is to supplement UV filtration with AVDs as follows:
1) Use AVDs during the R&D cycle to verify that UV filtration systems are performing as designed.
2) Deploy AVDs as real-time monitoring devices for UV filtration systems by incorporating two AVDs into the final product (one AVD ahead of the UV filter and one behind it).
3) Incorporate visual and audio devices into the UV filtration casing:

- **Green**: all systems are working as expected.
Passengers should use social distancing.

- **Yellow**: primary AVD detected COVID in an air duct inlet.
Light audio "ding" every 30 seconds.
Passengers should be aware of their immediate surroundings and observe rigid social distancing protocols.

- **Red**: secondary AVD detected COVID in an air duct outlet.
Light audio buzzer every 15 seconds.
Passengers should be aware of a UV filtration system malfunction and that social distancing is no longer effective.

Preventing station access

AVDs could be used to prevent access to ticket vending machines, shutdown infected TVMs and alert station staff when disinfection is required.
Fare gates could also be enhanced to prevent COVID-infected passengers from entering the system.

Funding

The Federal Emergency Management Agency (FEMA) should be responsible for funding R&D and deployment of devices designed to ensure the safety of passengers.

I hope you find this information useful.

Roland Lebrun.

CC
SF MUNI Board of Directors
SFCTA Commissioners
Caltrain Board
VTA Board of Directors
MTC Board of Directors
MUNI CAC
Caltrain CAC
SFCTA CAC
VTA CAC

Open Access | Published: 08 December 2015

Detection of airborne viruses using electro-aerodynamic deposition and a field-effect transistor

Kyu-Tae Park, Dong-Guk Cho, Ji-Woon Park, Seunghun Hong & Jungho Hwang

Scientific Reports **5**, Article number: 17462 (2015)

Abstract

We report a technique for the detection of aerosolized viruses. Conventional field-effect-transistor (FET)-based techniques use solution-based processes, thus require antibody binding to the detection region of the FET prior to the supply of the analyte. With the method described here, virus–antibody-bound particles are delivered to the FET during detection; therefore, neither a pre-treatment antibody binding step on the FET channel nor washing

process for virus–antibody-binding are necessary. Our method is based on the concept that virus–antibody-bound particles are larger than the virus or antibody alone and thus have larger charge numbers following aerosol charging. When these particles are charged by negative ions and electro-aerodynamically deposited on a substrate, there exists a location on the substrate where neither lone virus nor antibody particles land and where only virus–antibody-bound particles are deposited. If this location coincides with the channel of the FET, the resulting variation in the current can be used to indicate the existence of a virus. By aerosolizing a mixed solution of the virus and the antibody, only the virus–antibody-bound particles were transported to the swCNT-FET and the electric current in the swCNT-FET decreased to 30% of that measured with no deposited particles.

Introduction

Viruses are among the most important causes of human disease[1,2,3,4] and present a growing concern as potential agents for biological

warfare and terrorism[4,5]. Rapid, selective and sensitive detection of viruses is central to implementing an effective response to viral infections, such as through medication or quarantine. Established methods for viral analysis include plaque assays, immunological assays, transmission electron microscopy and polymerase chain reaction (PCR) testing for viral nucleic acids[3,6,7]. These methods, however, cannot achieve rapid detection of a single virus; moreover, they often require a relatively high level of sample manipulation, which is inconvenient with infectious materials. Nevertheless, the ability to rapidly, directly and selectively detect individual virus particles would have a marked impact on healthcare by enabling diagnosis at the earliest stages of replication within a host system.

Exposure to biological aerosols (bioaerosols), such as those from H1N1 influenza, severe acute respiratory syndrome (SARS)[8], bird flu[9] and bioterrorism attacks[10], has resulted in huge human and economic costs. Furthermore, the sustained growth in international travel increases the risk that an infectious disease may develop into a pandemic. These threats necessitate real-time bioaerosol sensing systems; however, development of such systems remains a

challenge. Technologies including bioaerosol mass spectrometry (BAMS)[11], surface-enhanced Raman spectroscopy (SERS)[12] and flow cytometry with fluorochrome[13] have been developed to detect bioaerosols. Fluorescence-based instruments, such as the ultraviolet aerodynamic particle sizer (UVAPS)[14,15], BioTrak®[16] and fluorescent microscopy with an inertial impactor[17] can optically measure concentrations of total and/or viable particles in real-time. However, these techniques are not capable of species-level discrimination and/or produce high false-positive rates[18]. Surface plasmon resonance and Mie scattering with aerosol sampling have been also used for bioaerosol detection[19,20]. However, these methods need pre-treatments for binding antibody on a surface or particles.

A promising approach to the direct electrical detection of viruses is the use of field-effect transistors (FETs). Following recent advances in technology, the importance of high-performance electronic devices has increased. FETs are one of the most important components of current semiconductor technology and have been applied in diverse fields outside of microelectronics. Such cross-disciplinary developments in technology provide an exciting

opportunity for environmental sensing applications. FETs have been successfully applied to the detection of biological species in liquids via translating virus binding events into electrical signals. Changes in the conductance of the channel of a FET due to selective binding of specific proteins or nucleic acid sequences at the device surface have been reported using purified samples[21,22,23]. In addition, the considerable progress that has been made in microfluidic channels has enabled the efficient transport of virus-laden liquids onto specific-antibody-coated FETs[20].

Current virus detection techniques that employ FETs are typically employing solution-based processes and require the application of an antibody-binding process to the FET channel prior to the detection process (Fig. 1A). With such an antibody binding process, chemical treatment of the FET channel is carried out, followed by washing (Fig. 1A-a). A solution containing antibody particles for the target virus is then supplied to the FET channel (Fig. 1A-b). The reaction between the FET channel and antibody particles typically requires between 10 minutes and 3 hours. Following another washing step (Fig. 1A-c), the target virus-laden liquid (obtained by an aerosol sampling technique of

capturing airborne viruses into a solution) is delivered to the FET to enable binding of virus particles onto the antibody particles (Fig. 1A-d). Then, another washing step is required to eliminate unbound virus particles (Fig. 1A-e). The presence of the bound virus particles changes the electrical characteristics of the FET, thereby implicating the existence of the virus (Fig. 1A-f).

Figure 1

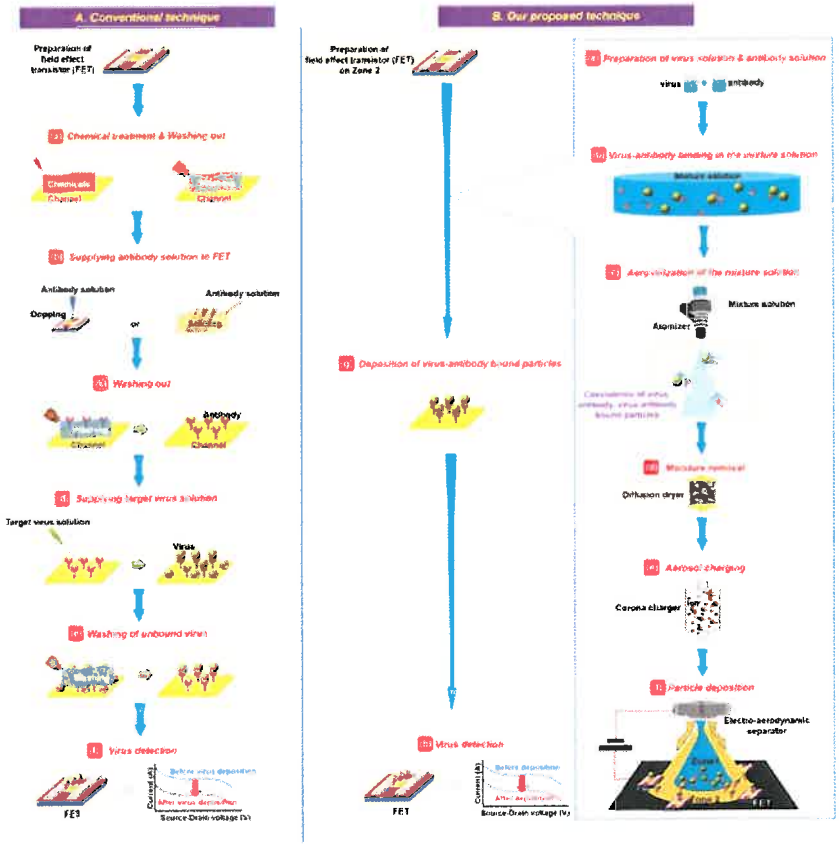

Electrical detection of the target virus using a specific antibody (K. –T. Park drew the figure by using Microsoft PowerPoint).

Here we report a technique for the electrical detection of airborne virus particles without pre-treatment, without requiring antibody–antigen binding and with no washing process involved in virus–antibody binding (Fig. 1B). Our method is based on the concept that both a virus and an antibody are particles of finite sizes. To realize our technique, a solution containing a target virus and another solution containing a specific antibody for this virus (Fig. 1B-a) must be prepared in advance, so that virus–antibody binding can occur (Fig. 1B-b). By atomizing the resulting mixture, the virus–antibody bound particles are aerosolized, as well as individual virus and antibody particles in the mixture solution (Fig. 1B-c). Water vapor and water droplets were removed by passing the aerosol flow through a diffusion dryer (Fig. 1B-d). The virus, antibody and virus–antibody aerosols were electrically charged using a corona discharge (Fig. 1B-e), after which they pass through a nozzle and then toward the substrate (Fig. 1B-f). An external electric field is applied between the nozzle and substrate. With this electro-aerodynamic (EAD) deposition[24], the motion of the particles is determined by inertial and electrical forces.

The smaller particles (i.e., virus and antibody)

have relatively low charge numbers, whereas large particles (i.e., virus–antibody bound particles) have larger charge numbers[25]. Owing to the differences in size and charge, the smaller particles are deposited at locations nearer the flow-impinging zone (hereafter referred to as Zone 1), whereas the larger particles are deposited more widely across the substrate. Thus, there exists a location (hereafter referred to as Zone 2) where neither lone virus nor lone antibody particles land, rather where virus–antibody bound particles are deposited (Fig. 1B-g). The FET channel was located in Zone 2 and the change in source–drain current caused by the deposition of the virus–antibody bound particles was measured as an indicator of the presence of the virus (Fig. 1B-h). The effects of particle size on particle charge number and particle deposition width are mathematically explained in "Supplementary information"

Results and Discussion

Figure 2(a) shows an optical image of a pristine single-walled carbon nanotube FET (swCNT-FET), which was obtained using optical microscopy (Sunny, Korea). Source and drain (Au/Pd electrodes) and SiO_2 film functionalized

with octadecyltrichlorosilane (OTS) are clearly evident in the image. Atomic force microscopy (AFM) was used to reveal the CNT structures in the channel region. Figure 2(b) clearly shows CNTs, which form a 5-μm-wide and 20-μm-long channel aligned between the source and drain electrodes.

Figure 2

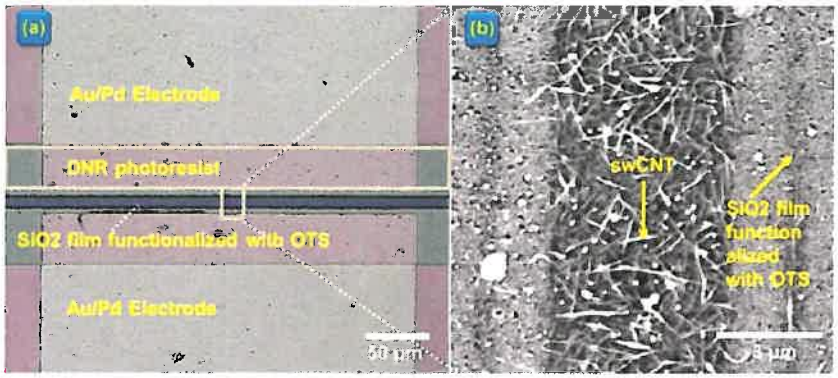

(**a**) Optical microscopy image of the swCNT-FET. (**b**) An AFM image of the swCNT channel region.

Stability and uniformity tests of the swCNT-FET were carried out. For the stability test, the temporal variation of source-drain current in the swCNT-FET was measured for 15 minutes and found to be negligible (Fig. 3 (a)). For the uniformity test, seventy-six swCNT-FET samples were fabricated and the distribution in conductance was measured. Figure 3 (b) shows that the distribution followed a log-normal

function, which is typical for percolating conductive networks[26,27] and that the conductance was between 5×10^{-8} S and 1×10^{-6} S for 88% of the samples.

Figure 3

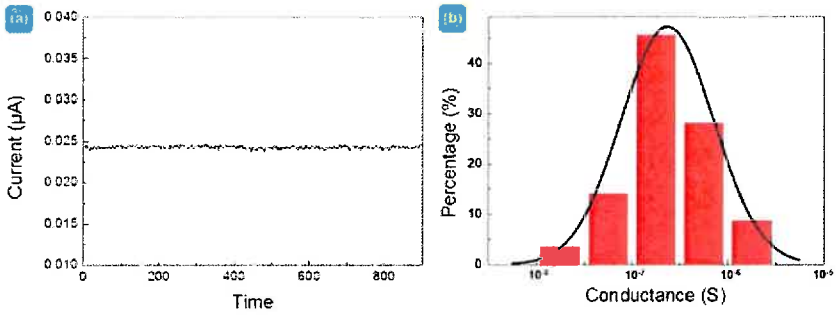

Stability and uniformity of swCNT-FETs; (a) Stability, (b) Uniformity.

The particle size distribution was measured following aerosolization of a solution containing virus and antibody particles and removal of moisture. Figure 4 shows three different size distributions obtained for solutions containing the MS2 bacteriophage virus, the antibodies for the MS2 bacteriophage and mixture of both particles. The quantity of virus particles in the virus solution was controlled to be the same as that of the antibody particles in the antibody solution. The virus, antibody and virus–antibody bound particles had modal diameters of 24 nm, 23 nm and 46 nm, respectively and the total

number concentrations were 6.7×10^5 #/cm^3, 6.72×10^5 #/cm^3 and 5.94×10^5 #/cm^3. Note that the virus and antibody particles were similar in size and thus similar in terms of the total number concentration. When the mixed solution was aerosolized, the particle size distribution shifted toward larger particles, as expected; however, the total number concentration decreased compared with that obtained using the virus solution or antibody solution. This may be due to the fact that polyclonal antibodies were used and so it is possible that unbound virus and antibody particles were present in the mixed solution.

Figure 4

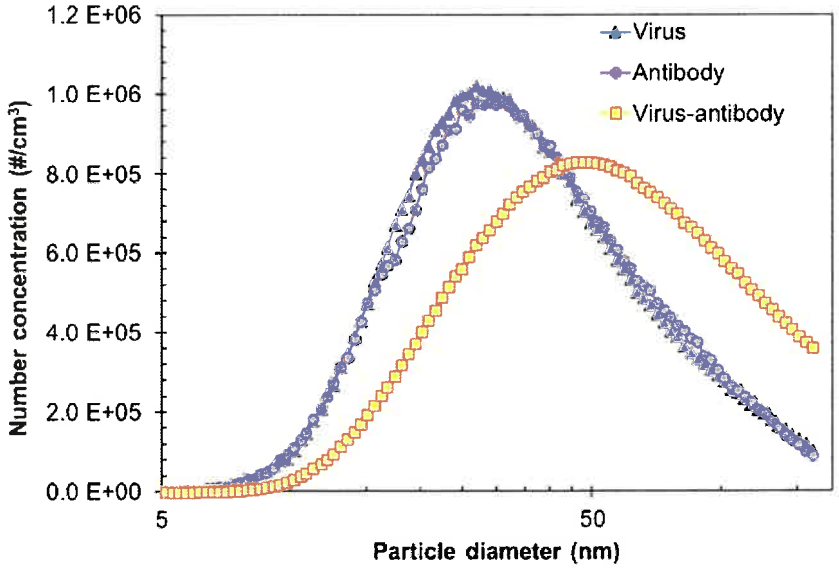

Size distributions of the virus, antibodies and virus–antibody bound particles.

The ratio of the number of virus particles to

antibody particles was 1:1.

After the particles were aerosolized, they were electrically charged using a corona charger. The charged particles entered the nozzle and were accelerated at the exit with a velocity of 1.17 m/s and impinged on the substrate. We have previously shown[24] that the deposition domain on the substrate is circular and that the diameter (or width) of the deposition domain is given by:

$$W_p = 1.92W(E_s)^{-0.41} \quad (1)$$

where W is the width of the nozzle width and E_s is the electrostatic number; i.e.,

$$E_s = \frac{neEC_c}{3\pi\mu dU} \quad (2)$$

where $e = 1.6 \times 10^{-19}$ C is the elementary charge, E is the electric field strength, μ is the viscosity of air, U is the air velocity at the nozzle, d is the particle diameter and C_C is the Cunningham slip correction factor; i.e.[25],

$$C_c = 1 + \frac{3\lambda}{d} \text{ for } d < 100\,\text{nm} \quad (3)$$

where λ is the mean free path of air molecules (66 nm). The average charge number of particles, n, was determined both theoretically and experimentally; details of this can be found in

the 'Methods' section.

The average charge numbers were calculated using Eq. (5) (see the 'Methods' section); these were 3.31 for the virus, 3.16 for the antibody and 6.63 for the virus–antibody bound particles. These numbers are in good agreement with those obtained experimentally using Eq. (4); i.e., 3.05, 2.97 and 6.79, respectively. Therefore, we found that the virus and antibody particles had a similar charge number in addition to their similar size.

The deposition widths for the aerosolized particles were calculated using Eq. (1); we find W_p = 14.1 mm for the virus, W_p = 13.9 mm for the antibodies and W_p = 17.4 mm for the virus–antibody bound particles. The deposition widths were measured using a digital camera (D80, Nikon, Japan). A black enclosure was installed near the deposition location to shield the region form external light. The measured deposition widths were 14.6 mm for the virus, 14.1 mm for the antibodies and 18 mm for the virus–antibody bound particles. Therefore, the measured data were in good agreement with the results of the calculations. Figure 5 also shows scanning electron microscope (SEM) images for four deposition spots. As shown in Fig. 5(a,b), the virus

and antibodies were deposited as single particles. Virus, antibodies and virus–antibody bound particles co-existed in Zone 1 ($W_p < 14.6$ mm; see Fig. 5(c1)); however, only virus–antibody bound particles existed in Zone 2 (14.6 mm $\leq W_p \leq 18$ mm; see Fig. 5(c2)). Therefore, the swCNT-FET channel was located in Zone 2 in subsequent experiments.

Figure 5

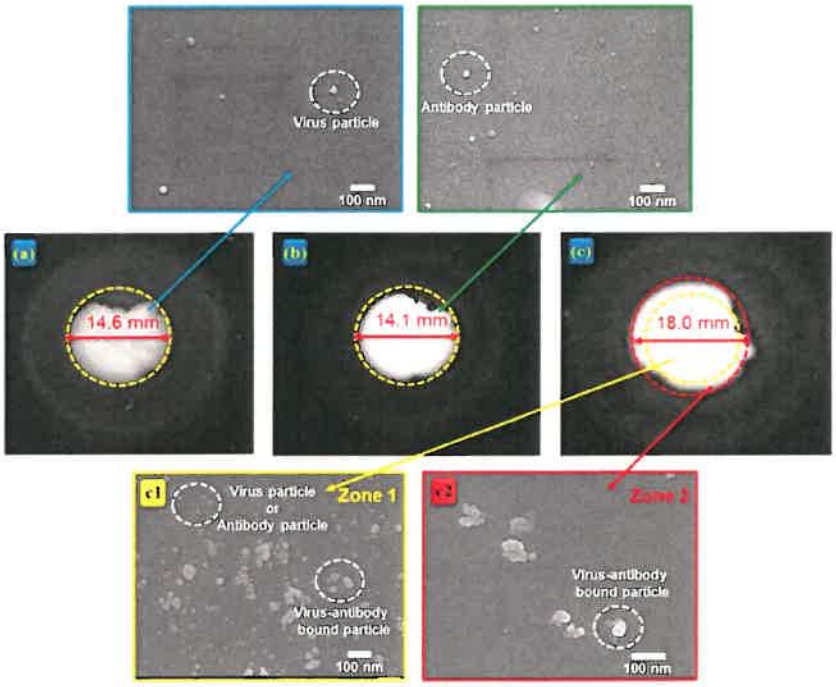

Photograph and SEM images of deposition spots using (**a**) a solution containing only the virus, (**b**) a solution containing only antibodies and (**c**) a mixed solution containing both virus and antibodies.

Additional experiments were carried out using antibodies specific for the H1N1 virus and not for the target bacteriophage MS2 virus. Figure 6(a) shows the size distribution of the aerosolized antibodies for the H1N1 virus. The particles had a modal diameter of 11 nm and a total number concentration of 6.58×10^5 #/cm^3. A solution containing the target bacteriophage MS2 virus and antibodies for the H1N1 virus was prepared and aerosolized and the aerosolized particles were electro-aerodynamically deposited. The deposition width was 14.4 mm (Fig. 6(b)), which is almost identical to that for the virus deposition shown in Fig. 5(a). Figure 6(c) shows an SEM image of deposition; single particles can be seen deposited on the substrate and particle agglomeration was not observed. It follows that no change in the size of the particles due to binding between the target bacteriophage MS2 virus and the antibodies for H1N1 occurred.

Figure 6

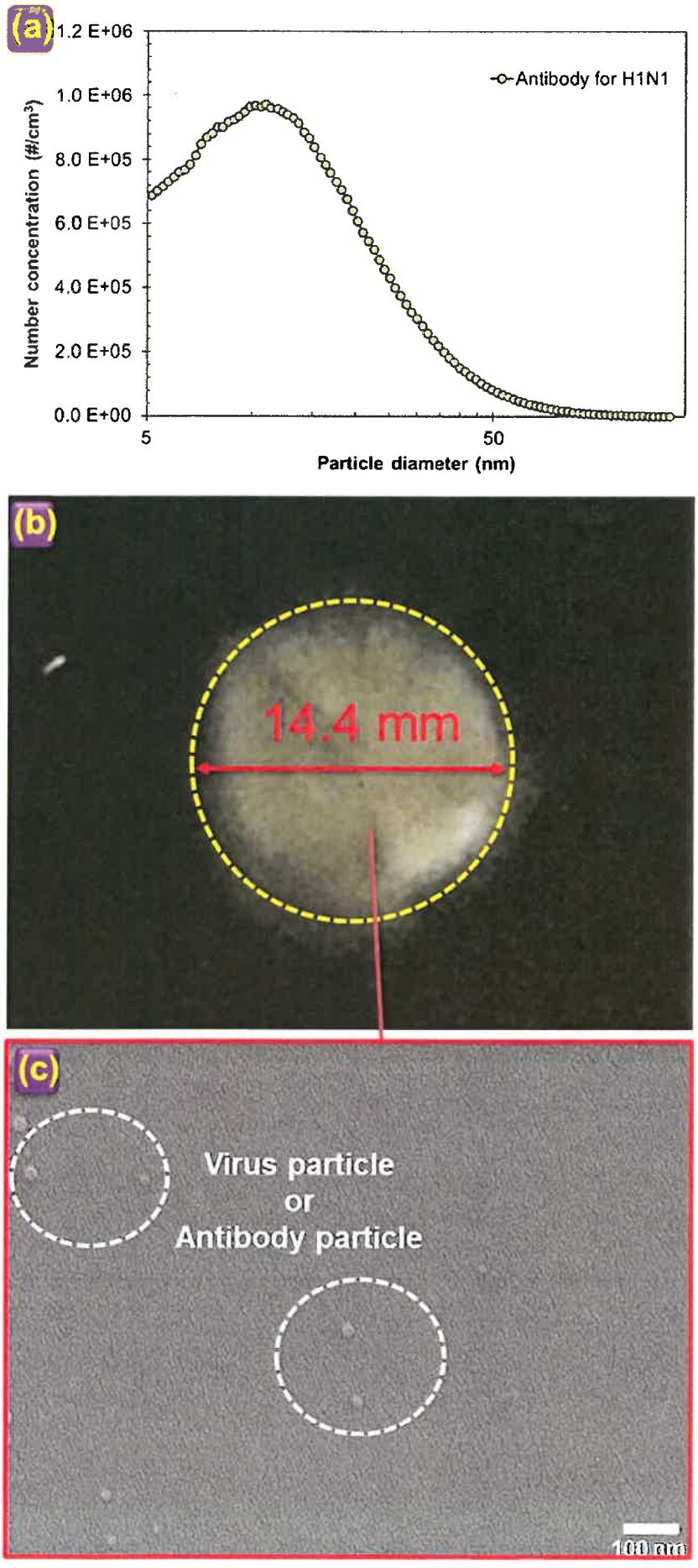

(**a**) The size distribution of the H1N1 antibodies.

(**b**) A photograph of deposition location. (**c**) An SEM image of the deposited particles.

Figure 7 shows the source–drain current as a function of the gate voltage (i.e., I-V characteristics of the swCNT-FET) before and after the deposition of the virus–antibody bound particles. Figure 7 shows a dramatic decrease in the current following deposition of virus–antibody bound particles. When the number concentration ratio of virus to antibody was 1:0 or 0:1, the current did not change from that measured with no particle deposition (control value). However, when the ratios were 0.01:1, 0.05:1 and 0.1:1, the current decreased to 93%, 87% and 46% of the control value, respectively, supporting that only virus-antibody bound particle can affect the current change. When the ratio further increased to 1:1 or 10:1, the current decreased to 30% of the control value on account of the higher number concentration of virus particles.

Figure 7

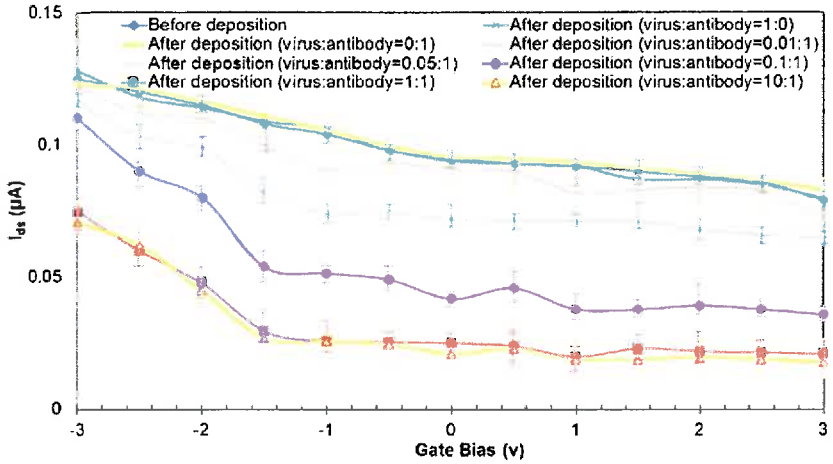

I-V characteristics of the swCNT-FET before and after the deposition of MS2 bacteriophage virus–MS2 bacteriophage antibody bound particles.

Detection of H1N1 virus was carried out to check the universality of our proposed method. The H1N1 virus, antibody for H1N1 and virus–antibody bound particles had modal diameters of 21.5 nm, 11 nm and 31 nm, respectively and the total number concentrations were 6.81×10^5 #/cm^3, 6.58×10^5 #/cm^3 and 5.83×10^5 #/cm^3. The charge numbers for H1N1 virus, antibody for H1N1 and virus-antibody bound particles were 2.85, 1.44 and 4.31, respectively. Since the calculated deposition widths were 13.3 mm, 10.7 mm and 15.7 mm, respectively, for H1N1 virus, antibody for H1N1 virus and virus-antibody bound particles, the swCNT-FET channel was located in the domain between 10.7 mm and 15.7

mm. Then particle deposition experiments were carried out and the change in source–drain current was observed. Figure 8 shows 20% decrease in the current after the deposition of the virus–antibody bound particles.

Figure 8

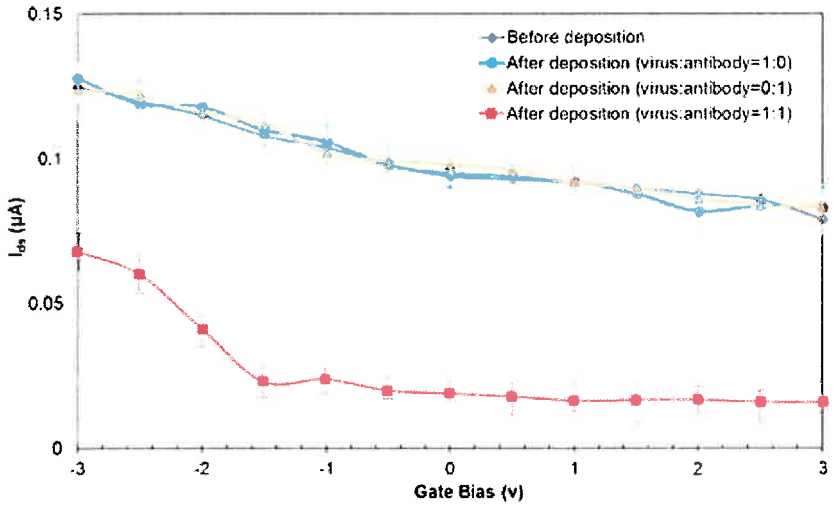

I-V characteristics of the swCNT-FET before and after the deposition of H1N1 virus–H1N1 antibody bound particles.

The reduced current in the swCNT-FET that was observed in the presence of virus–antibody bound particle was most likely due to donation of electrons from negatively charged virus–antibody bound particles (see Fig. S2 in "Supplementary information"). Because of the *p*-type characteristics of the swCNT, donation of electrons would reduce the number of holes (*p*-

type charge carriers) in the swCNT, resulting in a decrease in the source–drain current[28].

Conclusion

We have fabricated swCNT-FETs with an OTS SAM coating and demonstrated specific detection of aerosolized bacteriophage MS2 using anti-enterobacteriophage MS2 coat protein antibodies. Following deposition of the (negatively charged) virus–antibody bound particles on the p-type swCNT-FET channel, the source–drain current decreased to 30% of that measured with no particles deposition, which enabled detection of the presence of the target virus. Moreover, for the test of universality of our detection method, H1N1 virus was also detected and showed the source–drain current decreased to 20% of that measured with no particles deposition.

Methods

Fabrication of swCNT-FET

We fabricated FETs using p-type single-walled CNTs swCNTs. A suspension of swCNTs was prepared by dispersing 5 mg of swCNTs (Hanwha,

Korea) in 50 ml of 1,2-dichlorobenzene. To pattern the swCNT channel on a silicon dioxide wafer, an OTS self-assembled monolayer (SAM) technique was used. AZ5214 photoresist was patterned on the silicon oxide wafer using conventional photolithographic techniques. The wafer was then placed in a solution of OTS (1:500, v/v in hexane) for 5 min to form the OTS SAM on the wafer. The OTS-coated wafer was then dipped in acetone to remove the AZ5214 patterns, which resulted in an OTS-patterned wafer. The OTS-patterned wafer was then placed in the swCNT solution for 30 s and rinsed using 1,2-dichlorobenzene. The swCNTs were then selectively absorbed onto the bare silicon dioxide regions, whereas the OTS SAM regions blocked the absorption of the swCNTs. Source and drain electrodes (Au/Pd, 30 nm/10 nm) were fabricated using conventional photolithography, thermal evaporation and lift-off. The source and drain electrodes were passivated using photoresist. Further details of swCNT-FETs can be found in Lee *et al.*[29].

Preparation of the test virus, antibodies and mixed solutions

Bacteriophage MS2 (ATCC 15597-B1) and anti-enterobacteriophage MS2 coat protein antibody were used as the target virus and specific

antibody. Bacteriophage MS2 is commonly used in aerosol experiments as a surrogate for human and animal viruses[30]. Bacteriophage MS2 is nonpathogenic, can be prepared in high concentrations, is ideal for detection in aerosol experiments and responds to antimicrobial agents in a manner that is similar to human viruses[31].

Escherichia coli strain C3000 (ATTCC 15597) was selected as the host bacterium. To recover bacterial cells from a freeze-dried state, 10 ml of tryptic soy broth (TSB) were mixed with the freeze-dried bacterial cells. The mixture was incubated for 24 h at 37 °C with agitation. A total of 0.1 ml of the incubated bacterial solution was injected into another 10 ml of TSB. The TSB solution containing the bacteria was then used as the host bacterial solution following incubation for 6 h at 37 °C with agitation.

TSB (1 ml) was injected into the freeze-dried MS2 virus and 0.1 ml of the viral solution was extracted. The extracted solution was mixed with 0.3 ml of the host bacterial solution and 29 ml of soft tryptic soy agar (TSA), containing 8 g/l agar. The resulting agar solution was poured into a Petri dish and incubated overnight at 37 °C. The surface of the agar was removed using 10 ml of

phosphate-buffered saline (PBS) at pH 7.0. The solution was centrifuged for 20 min at 5,000 *g* and the supernatant was used as the virus solution in subsequent experiments. The virus solution was diluted using PBS to control the number concentration of the virus particles. Virus solutions with virus: antibody number concentrations of 0.01, 0.05, 0.1:1, 1:1 and 10:1 were prepared. Influenza A (H1N1) virus, strain A /Beijing/262/95 (8IN73-2, HyTest, Finland) was prepared for universality test. H1N1 virus solution was prepared with 10 ml of PBS and 120 μl of H1N1 virus stock,

Anti-enterobacteriophage MS2 coat protein antibodies (ABE76, Millipore, Germany) and monoclonal mouse anti-influenza virus type A (3IN5, HyTest, Finland) were used. The MS2 coat protein of bacteriophage is an RNA-binding protein that assembles into a pentameric structure to form the phage shell. The MS2 coat protein binds to a stem-loop structure in the viral RNA and facilitates packaging of RNA molecules into viral capsids. In addition, it represses synthesis of the viral replicase enzyme. The MS2 coat protein is widely used as an experimental model for the study of RNA–protein interactions that are involved in virus assembly. With the H1N1 antibodies, hybridoma

clones were derived from hybridization of Sp2/0 myeloma cells with spleen cells form BALB/c mice immunized with purified influenza virus type A strain H1N1. Two antibody solutions were prepared: one from 10 ml of PBS and 120 μl of anti-enterobacteriophage MS2 coat protein stock and the other from 2.5 ml of PBS and 195 μl of H1N1 antibody stock. The virus and antibody solutions were then mixed and incubated at room temperature for 10 min.

Experimental setup

Details of the experimental setup are shown in Fig. S3 of the 'Supplementary Information.' After the mixed solution was prepared, the particles were aerosolized using the following procedure. Compressed air was passed through a clean air supply consisting of an oil trap, a diffusion dryer and a high-efficiency particulate air (HEPA) filter. The particle-free compressed air then entered a Collison-type atomizer (9302, TSI Inc., USA), containing the mixture. The aerosol flow rate was controlled using a rotameter. Dry, clean air flowed at 2 lpm, forming a high-velocity jet through an orifice in the atomizer. The pressure drop from this jet was used to draw the mixed solution up through a tube, which was then broken into droplets due to the high-velocity air

jet. The resulting larger droplets impinged on an impactor, whereas the smaller droplets made no contact and formed an aerosol that exited through an outlet. The aerosolized mixed solution was passed through a diffusion dryer to remove water and a neutralizer (Soft X-ray charger 4530, HCT, Korea) to induce a Boltzmann charge distribution.

The neutralized particles entered a unipolar aerosol charger, with a stainless-steel needle (wire) electrode located at the center, which was used to generate a corona discharge at the sharp tip. The corona discharge generated air ions, which moved along the electric field to a grounded cylinder (made of duralumin). The charge per particle was controlled using a direct current (DC) voltage supplied from a high-voltage power supply. A bias of −8 kV was applied to the needle to charge the particles. Details of the charger are described in Park *et al.*[32].

The charged particles (i.e., virus, antibody, virus-antibody) then entered a 30-cm-long cylindrical nozzle (6 mm in diameter), which was used to induce a fully developed flow to minimize the entrance effect at the nozzle (which had a Reynolds number of Re = 700). The nozzle filet had a radius of curvature of 2 mm at the tip to

minimize the electric field[33]. After the charged particles were ejected from the nozzle, they were guided by an electric field and deposited on the substrate, which was located on an electrode that was biased at 7 kV. The separation between the nozzle and the substrate was 10 mm. The swCNT-FET was located where only the virus–antibody bound particles were deposited (i.e., in Zone 2).

The virus–antibody bound particles were deposited on the channel of the swCNT-FET, which led to a decrease in the source–drain current in the swCNT-FET. To measure the current, the swCNT-FET was connected to a semiconductor parameter analyzer (4200, Keithley, USA). A back-gated biasing method was used; the gate bias was varied in the range −3 V to + 3 V and a constant source–drain bias of 100 mV was applied.

Aerosol sampling was carried out upstream of the nozzle. A scanning mobility particle sizer (SMPS) system was used to characterize the size distribution of the particles, which consisted of a differential mobility analyzer (DMA, 3081, TSI, USA) and a condensation particle counter (CPC, 3025, TSI, USA), which could measure the diameter in the range 4–165 nm. The SMPS

system was operated with a sample flow rate of 0.3 lpm and a scan time of 180 s.

Average particle charge

The average particle charge was characterized by measuring the electric current resulting from the charged aerosol using an aerosol electrometer (3068A, TSI, USA), which consisted of a Faraday cup and an electrometer. Particles in the sample flow were collected in a high-efficiency conductive filter housed in a metal enclosure, which constituted the Faraday cup. Charged aerosols entered the instrument through an outer metal housing, which shielded the electrometer input from external electric fields. An absolute filter was used to remove the charged particles from the air stream, which was enclosed in an inner metal housing and electrically insulated from the outer metal housing. A signal feed connected the filter to the input of a solid-state electrometer amplifier. The electrometer had an analog output voltage range of 0–10 V, which corresponded to a maximum current of −12.5 to +12.5 pA. An ion trap was used to remove free unattached ions and to enable charged particles to pass through the ion trap zone, where the ion trap voltage was 200 V[34].

The average charge number of charged particles was calculated as follows:

$$n = \frac{I}{NeQ} \quad (4)$$

where I is the measured current, Q is the flow rate and N is the total number concentration of charged particles.

The average charge number was also calculated using the following expression[24]:

$$n \cong \frac{dk_BT}{2K_Ee^2} \ln\left[1 + \frac{\pi K_E d v_{i,rms} e^2 N_i t}{2k_BT}\right] \quad (5)$$

where $v_{i,rms} = 240$ m/s is the mean thermal speed of gaseous air ions, $K_E = 9.010^9$ Nm^2/C^2 is the electrostatic constant of proportionality, k_B is Boltzmann's constant, d is the mean particle diameter, T is temperature and $t = 0.0133$ s is the particle residence time. The concentration of corona-generated air ions was determined as follows:

$$Ni = \frac{I_C}{eZ_iEA} \quad (6)$$

where $I_C = 1.21 \times 10^{-7}$ A is the corona current, $Z_i = 1.6$ cm^2/Vs is the mobility of the gaseous ions and $A = 9.84 \times 10^{-7}$ m^2 is the internal surface area of the ground electrode.

Additional Information

How to cite this article: Park, K.-T. *et al.* Detection of airborne viruses using electro-aerodynamic deposition and a field-effect transistor. *Sci. Rep.* **5**, 17462; doi: 10.1038/srep17462 (2015).

References

1. Strauss, E., Strauss, J. & Strauss, E. G. Viruses and Human Disease. Academic, San Diego (2001).

2. Storch, G. A. Essentials of Diagnostic Virology, Churchill Livingstone, Edinburgh (1999).

3. Stadler, K. *et al.* Rappuoli, R. SARS — beginning to understand a new virus. Nat. Rev. Microbiol. 1, 209–218 (2003).

4. Atlas, R. M. Bioterrorism and biodefence research: changing the focus of microbiology. Nat. Rev. Microbiol. 1, 70–74 (2003).

5. Niiler, E. Bioterrorism—biotechnology to the rescue? Nat. Biotechnol. 20, 21–25

(2002).

6. Elnifro, E. M., Ashshi, A. M., Cooper, R. J. & Klapper, P. E. Multiplex PCR: optimization and application in diagnostic virology. Clin. Microbiol. Rev. 13, 559–570 (2000).

7. Mackay, I. M., Arden, K. E. & Nitsche, A. Real-time PCR in virology. Nucleic Acids Res. 30, 1292–1305 (2002).

8. Guan, Y. et al. Isolation and characterization of viruses related to the SARS coronavirus from animals in southern China. Science 302, 276–278 (2003).

9. Stone, R. Combating the bird flu menace. Down on the farm. Science 311, 944–946 (2006).

10. Enserink, M. How devastating would a smallpox attack really be? Science 296, 1592–1592 (2002).

11. Tobias, H. J. et al. Bioaerosol mass spectrometry for rapid detection of individual airborne Mycobacterium tuberculosis H37Ra particles. Appl. Environ. Microbiol. 71, 6086–6095 (2005).

12. Senguptaa, A., Brarb, N. & Davis, E. J. Bioaerosol detection and characterization by surface-enhanced Raman spectroscopy. J. Colloid Interface Sci. 309, 36–43 (2007).

13. Chen, P. S. & Li, C. S. Bioaerosol characterization by flow cytometry with fluorochrome. J. Environ. Monit. 7, 950–959 (2005).

14. Ho, J., Spence, M. & Fisher, G. Defense Research Establishment Suffield Report 619, (1995).

15. Agranovski, V., Ristovski, Z., Hargreaves, M., Blackall, P. J. & Morawska, L. Real-time measurement of bacterial aerosols with the UVAPS: performance evaluation. J. Aerosol Sci. 34, 301–317 (2003).

16. TSI hompage. http://www.tsi.com/biotrak-real-time-viable-particle-counter-9510-bd/ (accessed January 26, 2015).

17. Kang, J. S., Lee, K. S., Kim, S. S., Bae, G. N. & Jung, J. H. Real-time detection of an airborne microorganism using inertial impaction and mini-fluorescent microscopy. Lap Chip, 14, 244–251 (2014).

18. Shen, F. et al. Integrating silicon nanowire field effect transistor, microfluidics and air sampling techniques for real-time monitoring biological aerosols. Environ. Sci. Technol. 45, 7473–7480 (2011).

19. Usacheva, E. V., Usacheva, O. V. & Agranovski, I. E. Surface plasmon resonance-based real-time bioaerosol dtection, J. Appl. Microbiology, 115, 766–773 (2013).

20. Kwon, H. J., Fronczek, C. F., Angus, S. V., Nicolini, A. M. & Yoon, J. Y. Rapid and sensitive detection of H1N1/2009 virus from aerosol samples with a microfluidic immunosensor, J. Lab. Autom. 19, 322–331 (2013).

21. Cui, Y., Wei, Q., Park, H. & Lieber, C. M. Nanowire nanosensors for highly sensitive and selective detection of biological and chemical species. Science 293, 1289–1292 (2001).

22. Patolsky, F. et al. Electrical detection of single viruses. Proc. Natl. Acad. Sci. USA 101, 14017–14022 (2004).

23. Patolsky, F., Zheng, G. & Lieber, C. M.

Nanowire-based biosensors. Anal. Chem. 1, 4261–4269 (2006).

24. Park, J., Jeong, J., Kim, C. & Hwang, J. Deposition of charged aerosol particles on a substrate by collimating through an electric field assisted coaxial flow nozzle. Aerosol Sci. Technol. 47, 512–519 (2013).

25. Hinds, W. C. Aerosol technology: properties, behavior and measurement of airborne particle 2nd edn, Ch. 15, 320–331, (Wiley-Interscience, 1999).

26. Harris, A. B., Kim, S. & Lubensky, T. C. ε Expansion for the conductivity of a random resistor network. Phys. Rev. Lett. 53, 743–746 (1984).

27. Lee, B. Y. et al. Scalable Assembly Method of Vertically-Suspended and Stretched Carbon Nanotube Network Devices for Nanoscale Electro-Mechanical Sensing Components. Nano Lett. 8, 4483–4487 (2008).

28. Kim, J. Y., Lee, J., Hong, S. & Chung, T. D. Formaldehyde gas sensing chip based on single-walled carbon nanotubes and thin water layer. Chem. Commun. 47, 2892–2894 (2011).

ScienceDaily®
Your source for the latest research news

Science News *from research organizations*

A new biosensor for the COVID-19 virus

Detection in the environment

Date: April 21, 2020

Source: Swiss Federal Laboratories for Materials Science and Technology (EMPA)

Summary: Researchers have developed a novel sensor for detecting the new coronavirus. In future, it could be used to measure the concentration of the virus in the environment -- for example, in places where there are many people or in hospital ventilation systems.

Share:

FULL STORY

A team of researchers from Empa, ETH Zurich and Zurich University Hospital has succeeded in developing a novel sensor for detecting the new coronavirus. In future, it could be used to measure the concentration of the virus in the environment -- for example, in places where there are many people or in hospital ventilation systems.

Jing Wang and his team at Empa and ETH Zurich usually work on measuring, analyzing and reducing airborne pollutants such as aerosols and artificially produced nanoparticles. However, the challenge the whole world is currently facing is also changing the goals and strategies in the research laboratories. The new focus: a sensor that can quickly and reliably detect SARS-CoV-2 -- the new coronavirus.

But the idea is not quite so far removed from the group's previous research work: even before the COVID-19 began to spread, first in China and then around the world, Wang and his colleagues were researching sensors that could detect bacteria and viruses in the air. As early as January, the idea of using this basis to further develop the sensor in such a way that it could reliably identify a specific virus was born. The sensor will not necessarily replace the established laboratory tests, but could be used as an alternative method for clinical diagnosis, and more prominently to measure the virus concentration in the air in real time: For example, in busy places like train stations or hospitals.

Fast and reliable tests for the new coronavirus are urgently needed to bring the pandemic under control as soon as possible. Most laboratories use a molecular method called reverse transcription polymerase chain reaction, or RT-PCR for short, to detect viruses in respiratory infections. This is well established and can detect even tiny amount of viruses -- but at the same time it can be time consuming and prone to error.

An optical sensor for RNA samples

Jing Wang and his team have developed an alternative test method in the form of an optical biosensor. The sensor combines two different effects to detect the virus safely and reliably: an optical and a thermal one.

The sensor is based on tiny structures of gold, so-called gold nanoislands, on a glass substrate. Artificially produced DNA receptors that match specific RNA sequences of the SARS-CoV-2 are grafted onto the nanoislands. The coronavirus is a so-called RNA virus: Its genome does not consist of a DNA double strand as in living organisms, but of a single RNA strand. The receptors on the sensor are therefore the complementary sequences to the virus' unique RNA sequences, which can reliably identify the virus.

The technology the researchers use for detection is called LSPR, short for localized surface plasmon resonance. This is an optical phenomenon that occurs in metallic nanostructures: When excited, they modulate the incident light in a specific wavelength range and create a plasmonic near-field around the nanostructure. When molecules bind to the surface, the local refractive index within the excited plasmonic near-field changes. An optical sensor located on the back of the sensor can be used to measure this change and thus determine whether the sample contains the RNA strands in question.

Heat increases reliability

However, it is important that only those RNA strands that match exactly the DNA receptor on the sensor are captured. This is where a second effect comes into play on the sensor: the plasmonic photothermal (PPT) effect. If the same nanostructure on the sensor is excited with a laser of a certain wavelength, it produces localized heat.

And how does that help reliability? As already mentioned, the genome of the virus consists of only a single strand of RNA. If this strand finds its complementary counterpart, the two combine to form a double strand -- a process called hybridization. The counterpart -- when a double strand splits into single strands -- is called melting or denaturation. This happens at a certain temperature, the melting temperature. However, if the ambient temperature is much lower than the melting temperature, strands that are not complementary to each other can also connect. This could lead to false test results. If the ambient temperature is only slightly lower than the melting temperature, only complementary strands can join. And this is exactly the result of the increased ambient temperature, which is caused by the PPT effect.

To demonstrate how reliably the new sensor detects the current COVID-19 virus, the researchers tested it with a very closely related virus: SARS-CoV. This is the virus that broke out in 2003 and triggered the SARS pandemic. The two viruses -- SARS-CoV and SARS-CoV2 -- differ only slightly in their RNA. And validation was successful: "Tests showed that the sensor can clearly distinguish between the very similar RNA sequences of the two viruses," explains Jing Wang. And the results are ready in a matter of minutes.

At the moment, however, the sensor is not yet ready to measure the corona virus concentration in the air, for example in Zurich's main railway station. A number of developmental steps are still needed to do this -- for example, a system that draws in the air, concentrates the aerosols in it and releases the RNA from the viruses. "This still needs development work," says Wang. But once the sensor is ready, the principle could be applied to other viruses and help to detect and stop epidemics at an early stage.

Story Source:

Materials provided by **Swiss Federal Laboratories for Materials Science and Technology (EMPA)**. Original written by Karin Weinmann. *Note: Content may be edited for style and length.*

Journal Reference:

1. Guangyu Qiu, Zhibo Gai, Yile Tao, Jean Schmitt, Gerd A. Kullak-Ublick, Jing Wang. **Dual-Functional Plasmonic Photothermal Biosensors for Highly Accurate Severe Acute Respiratory Syndrome Coronavirus 2 Detection**. *ACS Nano*, 2020; DOI: 10.1021/acsnano.0c02439

Cite This Page:

MLA APA Chicago

Swiss Federal Laboratories for Materials Science and Technology (EMPA). "A new biosensor for the COVID-19 virus: Detection in the environment." ScienceDaily. ScienceDaily, 21 April 2020. <www.sciencedaily.com/releases/2020/04/200421112520.htm>.

RELATED STORIES

Carbon Dioxide Sensor Can Lower Energy Use, Reduce Utility Costs

Apr. 22, 2020 — Researchers developed a sensor to help control and cut down on energy consumption through heating and ventilation ...

Cost-Effective Canopy Protects Health Workers from COVID Infection During Ventilation

Apr. 20, 2020 — Researchers have designed a cost-effective, plastic canopy system that can help to protect healthcare workers who are at risk of airborne coronavirus infection while delivering noninvasive ...

An App Knows If a Beer Has Gone Stale

May 19, 2016 — Chemists have developed a method that allows brewers to measure the freshness of beer, using a polymer sensor that changes color upon detecting furfural, a compound that appears when this beverage ...

Using Drones for Better Crops

July 13, 2015 — A new study has used a drone to measure the temperature, humidity, luminosity and

carbon dioxide concentration in a greenhouse. The capacity of an aerial vehicle to move in three-dimensional space ...

Follow Us

Keep up to date with the latest news from ScienceDaily via social networks:

- Facebook
- Twitter
- LinkedIn

Have Feedback?

Tell us what you think of ScienceDaily -- we welcome both positive and negative comments. Have any problems using the site? Questions?

- Leave Feedback
- Contact Us